JOURNAL OF Applied Polymer SCIENCE

Effect of Core-Shell Morphology Evolution on the Rheology, Crystallization, and Mechanical Properties of PA6/EPDM-*g*-MA/HDPE Ternary Blend

Rui Dou, Wei Wang, Yan Zhou, Lan-peng Li, Lei Gong, Bo Yin, Ming-bo Yang

State Key Laboratory of Polymer Materials Engineering, College of Polymer Science and Engineering, Sichuan University, Chengdu, Sichuan, China

Correspondence to: B. Yin (E-mail: yinbo@scu.edu.cn)

ABSTRACT: In this article, polyamide 6 (PA6), maleic anhydride grafted ethylene-propylene-diene monomer (EPDM-*g*-MA), high-density polyethylene (HDPE) were simultaneously added into an internal mixer to melt-mixing for different periods. The relationship between morphology and rheological behaviors, crystallization, mechanical properties of PA6/EPDM-*g*-MA/HDPE blends were studied. The phase morphology observation revealed that PA6/EPDM-*g*-MA/HDPE (70/15/15 wt %) blend is constituted from PA6 matrix in which is dispersed core-shell droplets of HDPE core encapsulated by EPDM-*g*-MA phase and indicated that the mixing time played a crucial role on the evolution of the core-shell morphology. Rheological measurement manifested that the complex viscosity and storage modulus of ternary blends were notable higher than the pure polymer blends and binary blends which ascribed different phase morphology. Moreover, the maximum notched impact strength of PA6/EPDM-*g*-MA/HDPE blend was 80.7 KJ/m^2 and this value was 10–11 times higher than that of pure PA6. Particularly, differential scanning calorimetry results indicated that the bulk crystallization temperature of HDPE (114.6°C) was partly weakened and a new crystallization peak appeared at a lower temperature of around 102.2°C as a result of co-crystal of HDPE and EPDM-*g*-MA. © 2012 Wiley Periodicals, Inc. J. Appl. Polym. Sci. 129: 253–262, 2013

KEYWORDS: morphology; crystallization; rheology; mechanical properties; polyamides

Received 13 July 2012; accepted 14 October 2012; published online 6 November 2012
DOI: 10.1002/app.38733

INTRODUCTION

It has been a long-standing interest of polymer researchers in understanding the evolution of phase morphology and a relative more effort is still devoting to the regulation and evolution of phase microstructure by now. Generally the phase morphology depends on several parameters. These are chemical and physical interactions, interfacial tension, processing conditions, coalescence phenomena, and rheological characteristics of the polymeric immiscible phases.[1–6] Two types of common morphologies usually form in immiscible binary blends, that are, the sea-island morphology and the co-continuous morphology.[7–10] Concerning the phase morphology containing multiphase dispersed in polymer matrix, droplet-matrix morphology and core-shell microstructure are the two morphologies commonly observed in ternary polymer blends. The phase structure can be stabilized when the system being the one with the lowest interfacial free energy, the opportunity for one minor phase to encapsulate another minor component in ternary blends can be estimated by eq. (1):[11]

$$\lambda_{31} = \delta_{12} - \delta_{32} - \delta_{13}. \quad (1)$$

Where δ_{12}, δ_{32} and δ_{13} are the interfacial tension for each component pair, and λ_{31} is the spreading coefficient for component 3 (shell) to encapsulate component 1 (core). The index 2 refers to the matrix, λ_{31} must be positive for 1 to be encapsulated by 3. Some researchers have designed core-shell morphology of ternary blends via controlling of component ratio of minor phases.[12–14] In our previous research work, it was found that core-shell morphology of polymer blends could be controlled by changing processing methods.[14,15] Furthermore, the formation and evolution of core-shell morphology is also affected by other factors such as the melt viscosity, torque ratio, process parameters, compatibilization, elasticity etc.[16–21]

As we know there exists a remarkable parallelism between the mechanical properties and the phase morphology of polymer blends. The satisfactory toughening effects of poly (lactic acid) (PLA) often depends on the balance between interfacial compatibilization and crosslinking of the elastomer.[22] Also according to the framework of Wu's theory, the brittle-ductile transition of blend depends on the particle size and inter-particle distance.[23] Now many researchers have paid attention to optimizing the

mechanical properties of blends containing core-shell microstructure dispersed in a polymer matrix. Luzinov etc.[24] focused on the morphology and mechanical properties of ternary blends consisting of polystyrene matrix and polyolefin/styrene butadiene rubber core-shell dispersed phases. The ultimate mechanical properties of the blends show some dependence on the stiffness of the PO core according to their conclusion. The mechanical properties and the morphologies for ternary blends of a core-shell structure with a low density polyethylene core and an elastic polybutadiene shell in Polyamide 6 (PA6) matrix was studied by Zhuo Ke etc.[25] For blend with 90 wt % PA and 10 wt % core-shell toughener, they found that there was only a 10 % loss in modulus but a 10-fold increase in impact toughness compared to neat PA6. Also the use of core-shell structure for impact modification of polypropylene,[26] polymethyl methacrylate,[27] polybutylene terephthalate,[28] poly(trimethylene terephthalate)[29] has been reported by a number of researchers with varied success.

However, most previous work was focused on the research of modifying materials while the effect of core-shell structure evolution (such as interface entanglement, phase size, particle distribution, etc.) on rheology properties, crystallization behavior of polymer blend had not been paid more attention. In our article, PA6, ethylene-propylene-diene monomer (EPDM-*g*-MA) and High density polyethylene (HDPE) were melt blended for various time to study the morphology evolution based on the migration of EPDM-*g*-MA. In this ternary blend, the morphology of PA6 as a matrix with HDPE encapsulated within the dispersed EPDM-*g*-MA was obtained after melt-mixing which has been reported by Li etc.[14] and the relationship between impact toughness and the morphology of the blend was investigated. Moreover, the rheological behavior of the ternary blend was discussed to elucidate the core-shell structure evolution. The crystallization behaviors of HDPE and PA6 were studied by employing differential scanning calorimetry (DSC). Specially, the unexpected crystallization behavior of HDPE phase may have provided us with new insights into the toughening mechanism of ternary blend containing core-shell morphology.

EXPERIMENTAL PART

Materials

PA6 resin used here, with the grade AKULON F136-C, was supplied by DSM, Netherland, having a melt viscosity of 547.1 Pa·s (240°C, 100 1/s) and a density of 1.13 g/cm^3. Maleic anhydride grafted EPDM-*g*-MA, with the trademark Bondyram® 7003, was purchased from Bondyram, Israel, it has a melt viscosity of 396.7 Pa·s (240°C, 100 1/s) and had been grafted with 0.7 wt % maleic anhydride group. HDPE was 6098 grade from Qilu Petrochemical Company Ltd, China, with a mass density of 0.95 g/cm^3 and a melt viscosity of 436.9 Pa·s (240°C, 100 1/s). All these materials are commercial available.

Blends Preparation

Before blending, PA6 was dried in a vacuum oven for 24 h at 80°C. All the blends were prepared by adding the raw materials simultaneously in an internal mixer of a HAAKE torque rheometer at a temperature of 230°C, with a rotor speed of 30 rpm. All experiments were conducted under a nitrogen atmosphere to minimize oxidative degradation of the polymer blends. PA6/EDPM-*g*-MA, PA6/HDPE binary blends were mixed for about 5 min until a constant torque value reached and the neat polymers used as for reference samples were obtained under the same conditions. Moreover, PA6/EDPM-*g*-MA/HDPE ternary blends, with a constant composition ratio of 70/15/15, were prepared by mixing under a series of different times. The detail information of the samples was listed in Table I (All ratios in this article represent weight ratio).

Table I. Designation and Composition of the Blends

Code	Composition (blend ratio)	Mixing time (min)
P85H15	PA6/HDPE-85/15	5
P85M15	PA6/EPDM-*g*-MA-85/15	5
PMH2	PA6/EPDM-*g*-MA/HDPE-70/15/15	2
PMH5	PA6/EPDM-*g*-MA/HDPE-70/15/15	5
PMH8	PA6/EPDM-*g*-MA/HDPE-70/15/15	8
PMH10	PA6/EPDM-*g*-MA/HDPE-70/15/15	10
PMH15	PA6/EPDM-*g*-MA/HDPE-70/15/15	15

Tests and Characterizations

Phase Morphology Characterization. A JEOL JSM-5900LV scanning electron microscopy (SEM, JEOL, Japan) at a 20 kV accelerating voltage was used to observe the phase morphology of the blends. The samples were cryo-fractured in liquid nitrogen and the fractured surfaces were sputtered with gold before observation. In some cases, the cryogenically fractured surface was etched with xylene to remove the EPDM-*g*-MA so as to emphasize the contrast between phases.

Quantitative analysis of the morphology was performed using image analysis of Image-Pro Plus 6. At least 300 dispersed domains were measured by manually tracing the phase boundaries to estimate the number-average diameter for each sample.

Rheological Measurements. The dynamic viscoelastic behaviors of each sample was studied using an AR2000ex stress controlled dynamic rheometer (TA Corporation, USA) using a parallel plate geometry with 25 mm diameter. In order to prevent thermo-oxidative degradation, all experiments were performed under nitrogen atmosphere. Disks of 25 mm diameter and 1 mm thickness were molded at 240°C, under a pressure of 10 MPa for 3 min. During the rheological measurement process, the frequency sweep from 0.01 to 100 rad/s was performed at 240°C under dry nitrogen atmosphere. The strain used was 2 % which ensures to be in the linear regime.

Differential Scanning Calorimetry (DSC). DSC measurements were performed on a TA Instrument model DSC Q20 under nitrogen gas flow. About 6 mg samples encapsulated into aluminium pans were submitted to cooling and heating cycles.

Standard DSC test. Samples were quickly heated to 250°C with a heating rate of 100°C/min and held at 250°C for 5 min to erase thermal history, and then cooled to 40°C at 10°C/min and held at 40°C for 1 min. Finally, the samples were heated to

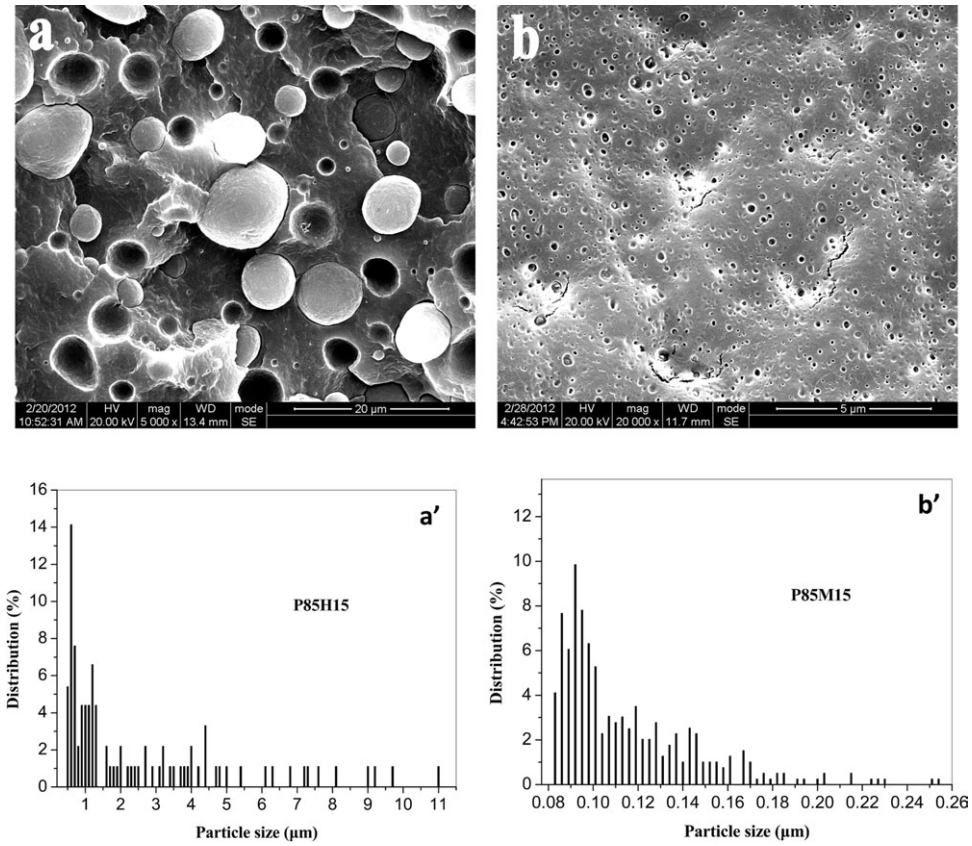

Figure 1. Morphology of cryo-fractured surface of binary blends: (a) P85H15, (b) P85M15, (a', b') particle size distribution.

250°C again at 10 °C/min. The crystallization curve and the second melting curve were recorded.

The successive self-nucleation and annealing (SSA) test. SSA was first presented in 1997 by Müller etc.[30] In our experiment, in order to analyze the thermal fractionation of HDPE, samples were firstly heated to 160°C at 100°C/min and kept at this temperature for 5 min to erase thermal history, subsequently down to 40°C at 10°C/min to create a "standard" thermal history; then samples were heated to first self-seeding temperature of 135°C at 10°C/min and annealing at this temperature for 5 min. Crystallization after self-nucleation was achieved by subsequently cooling the samples to 40°C at 10°C/min. This cyclic procedure was repeated four times, and each self-nucleation annealing temperature was 5°C lower than the previous one. Finally the thermally treated samples were heated from 40°C to 160°C at 10°C/min and the corresponding endothermic curves were recorded.

Wide-angle X-ray Diffraction (WAXD). The crystalline structure of the composite was investigated at room temperature on a DX-1000 X-ray diffractometer (Dandong Fanyuan Company, China) with Cu Ka radiation of wavelength of 1.54 Å. The continuous scanning angle range used in this study was from 5° to 35° at 50 kV and 30 mA.

Izod Impact Strength Test. After the blends were taken out of the mixing chamber, cooled to ambient temperature and smashed with a pulverizer, the blends were dried and injection molded using a mini-injection molding machine (Thermo Scientific HAAKE Minijet, USA) into standard samples of 78 × 10 × 4 mm. Then the UJ-40 cantilever beam impact tester (Chengde Jinjian Testing Instrument Co. Ltd., Heibei, China) were employed for Izod test at a temperature of 0°C after the specimens notched at 45°C with a depth of 2 mm according to ASTM D256-05.[31] The direction of fracture propagation was perpendicular to the melt inject flow direction. The reported values for each composite were calculated as averages about 5-7 specimens.

RESULTS AND DISCUSSION

Morphology

Prior to the study of PA6/EPDM-*g*-MA/HDPE ternary blends, a complete view on the phase morphology development of the PA6/HDPE and PA6/EPDM-*g*-MA binary blends is necessary. Figure 1 shows the SEM micrographs and particle size distribution of the PA6/HDPE and PA6/EPDM-*g*-MA binary blends. As expected, the interfacial adhesion between HDPE particles and PA6 matrix [Figure 1(a)] is very poor in PA6/HDPE blend which is induced by the immiscibility of PA6 and HDPE.[32] For PA6/EPDM-*g*-MA blend, the holes on the fracture surface of the blend reflect the dispersed EPDM-*g*-MA phase [seen in Figure 1(b)]. In comparison to PA6/HDPE binary blend, the size of rubber particles are decreased which attributes to reaction between the carboxyl group in maleic anhydride of EPDM-*g*-

Applied Polymer SCIENCE

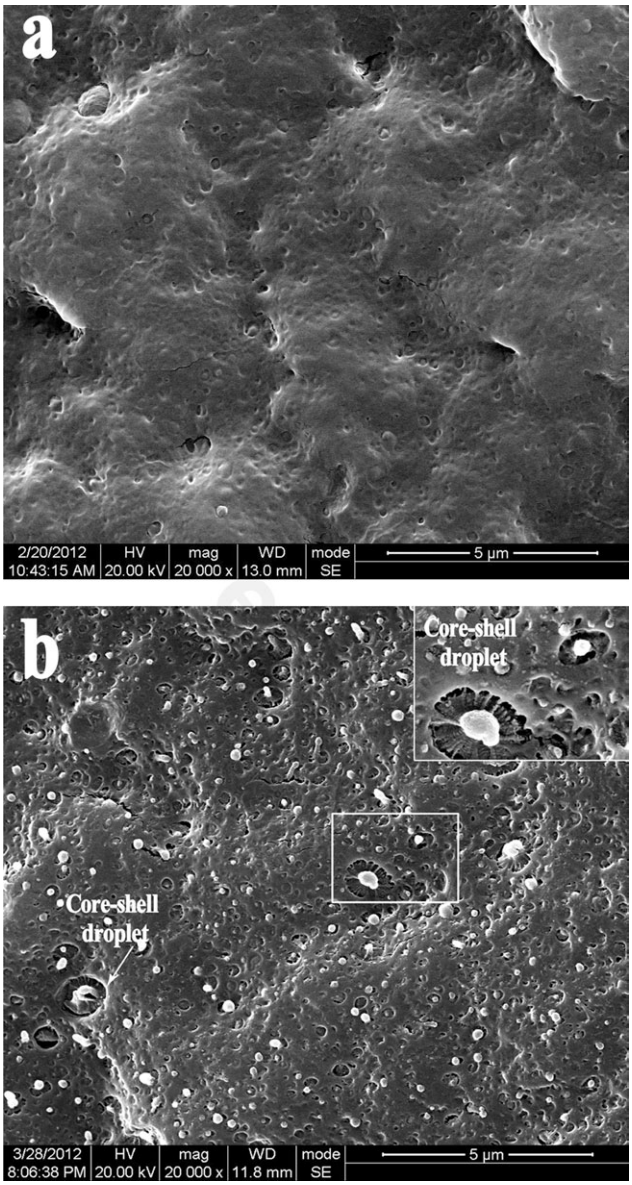

Figure 2. SEM micrographs of PMH5 ternary blend: (a) cryo-fractured surface, (b) cryo-fractured surface with EPDM-*g*-MA etched using xylene.

MA and the amino end group in PA6, and the refined interface of the two phases is resulted from inhibition of the coalesce of dispersed phases.[33,34]

The characterization of the phase morphology of PA6/EPDM-*g*-MA/HDPE blend is shown in Figure 2(a). A smooth fractured-surface and an indistinct phase interface between dispersed phases and matrix are observed in the ternary blend which indicates better interfacial adhesion between different phases. In order to enhance the comparison of different phases and clarify the multiphase structure, EPDM-*g*-MA was selectively etched using xylene. The cryo-fractured surface shown in Figure 2(b) reveals the existence of encapsulated droplets with an EPDM-*g*-MA shell and a HDPE core dispersed in PA6 matrix which has been reported in our previous work.[14] Also it is obvious that EPDM-*g*-MA locates at the interface and connects the PA6 and HDPE phase. Possibly it is both the reactive compatibility between PA6 and EPDM-*g*-MA and the partly miscible between EPDM-*g*-MA and HDPE that make a strong interface adhesion of different phases in PA6/EPDM-*g*-MA/HDPE blend.

For the purpose of clarifying the evolution mechanism of core-shell droplets in the ternary blend of PA6/EPDM-*g*-MA/HDPE, the compound mixed for various time with a constant constitute ratio was processed in a torque rheometer and the morphology of different samples can be observed in Figure 3. With a global morphology of the composites, it can be observed that the sizes of dispersed phase domains are gradually changing with varying levels by increasing the mixing time. Also it can be seen that the dispersed phase changes from a long threads [Figure 3(a)] to a uniform dispersed drop shape [Figure 3(b)] and then to a few bulky particles [Figure 3(c)] and similar result has been reported by Valera etc.[35] In order to show the effect of various mixing time on the size distribution of core-shell droplets more clearly, the particle size distribution and the values are displayed in Figure 3 (part a', b', c'). For the blends mixing with a shorter time (such as PMH5), the particle size is uniform and even the size distribution is narrower. With the mixing time increasing, the aggregation effect of dispersed particles can be increased due to long time mixing. As a result, a few of small particles tend to integrate into a larger one which leading to the size distribution becomes broader. Indeed, in the blend of PMH2 the dispersed phase has a broader size distribution, whereas in the same composition of PMH5 blend each particle size is less than 1μm and the size distribution is narrower. By mixing with a relatively long time for PMH15, majority of particles have a size of less than 0.5μm while a few ones tend to be larger which caused by favored coalescence [shown in Figure 3(c')].

The results indicated that EPDM-*g*-MA acted as an emulsifier enhancing the interface adhesion between PA6 and HDPE and reducing the diameter of HDPE dispersed phase.

Rheological Behavior

The viscoelastic property generally observed for multiphase polymer blends under small-amplitude oscillatory shear is the increase in elasticity at low frequencies and the appearance of a long relaxation time process. This behavior has been described in the literature by several emulsion-type models[36–38] and is ascribed to the deformability and the shape recovery ability of the dispersed particles due to the effect of interfacial tension effect. Generally, the shear viscosity of pure polymer is characterized by two distinct regions: the Newtonian region and the shear thinning region.[39] Figure 4(a) shows the complex viscosity curves of pure PA6, P85H15, P85M15, and PMH5. At low frequency range (for ω range from 0.01 Hz to 0.1 Hz), the PA6 behaves somewhat like a Newtonian fluid while for the P85H15 and P85M15 blend, the Newtonian region becomes weaker, and disappears for the PMH5 blend. The Storage modulus of these different blends is indicated in Figure 4(b). It is well known that the storage modulus reflects the elastic (solid-like) behavior of the polymer material at low frequency.[40] Blending EPDM-*g*-MA (which is already elastomer) to the P85M15 blend caused G′ to increase considerably, which is expected, compared with pure PA6 and P85H15 blend. At the same frequency, PMH5 displays a significant increase in G′. According to our precious

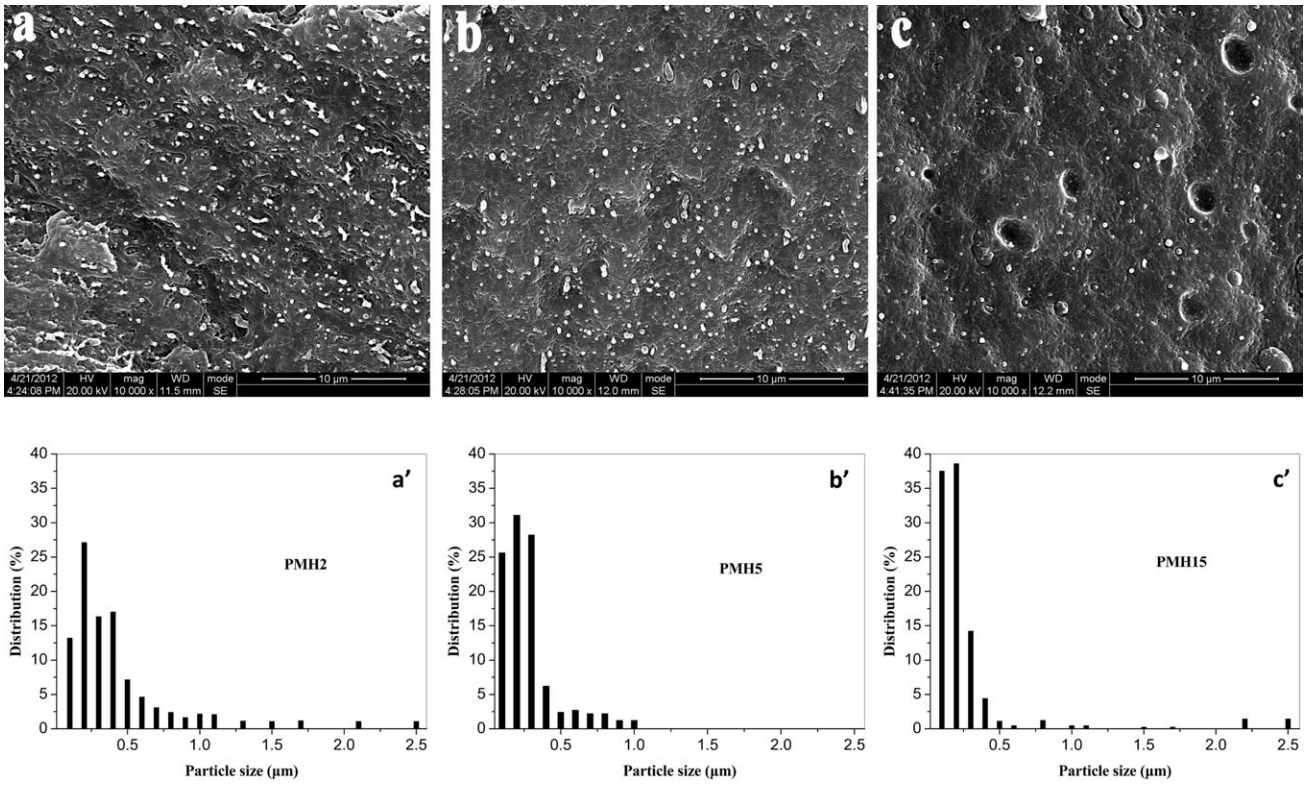

Figure 3. Morphology of cryo-fractured surface of different PA6/EPDM-*g*-MA/HDPE blends with EPDM-*g*-MA etched using xylene: (a) PMH2, (b) PMH5, (c) PMH15; (a', b', c') particle size distribution.

work,[14] in the multiphase system, the deformation and relaxation process of dispersed phase droplets will change the interface area of matrix/dispersed phase. So the increase of G′ for PMH5 is attributed to the effect of interfacial energy.

The storage modulus (G′) and loss tangent angle (tan δ) of different ternary blends are illustrated in Figure 5. It can be seen from the enlarged figure in Figure 5(a) that PMH5 exhibits a slightly larger value of G′ while PMH10 and PMH15 display a lower one. This is because more perfection and homogenous dispersion of core-shell droplets form in PMH5 which caused by strong interaction between core-shell droplets and matrix, and so under small-amplitude oscillatory shear dispersed particles have better recoverable ability from deformed state.[41,42] For PMH10 and PMH15 blend, the storage modulus decreases may be attributing to the decrease of surface energy caused by the effect of coalescent phenomenon. The same result can also obtain through analyzing tan δ showed in Figure 5(b).

Crystallization Behavior of HDPE and PA6

It has been reported by the Groeninckx and coworkers[43–46] that the crystallization behavior of dispersed droplets of minor phase can be affected by its microstructure and size. Figure 6 presents DSC thermograms of pure PA6, HDPE, and PA6/EPDM-*g*-MA/HDPE blend, from which values of crystallization peak temperature (T_c), melting peak temperature (T_m), and crystallinity (X_c) are all summarized in Table II.

In this article, pure PA6 and HDPE show T_c values of 190.1°C and114.6°C, respectively, also the T_c of PA6 phase for all the ternary blends maintains nearly invariant compared to that of the pure PA6 which can be attributed to the inconspicuous effect of core-shell droplets on the PA6 matrix. On the contrary, core-shell structure reveals significant influence on the crystallization behavior of HDPE phase. As is shown in Table II and Figure 6, for the ternary blends, compared with the constant crystallinity of PA6 component, largely decrease of X_c for HDPE was observed. Moreover unexpected double crystallization peaks are appeared at the range of 100°C to 115 °C for HDPE phase. The high temperature peak (T_{c1}) of all blends is observed at almost 114°C which represents the bulk crystallization peak temperature of HDPE phase and only the intensity of the exothermic peak becomes weaker. And the low temperature peak (T_{c2}) is monotonously moved to a lower temperature with the increasing of mixing time. For example, the T_{c2} is reduced from 104.9°C to 103.8°C, 102.2°C, 101.3°C to 100.7°C, when 2 min, 5 min, 8 min, 10 min, and 15 min mixing time are carried out, respectively. However, the exothermic peak intensity of T_{c2} becomes stronger. Undergoing sketchy analyses, this crystalline phenomenon is may be originated from partly compatibility of EPDM-*g*-MA and HDPE in melt state because both of them have a fraction of similar methylene segment which make EPDM-*g*-MA play a confined role on the HDPE according to the entanglement of molecule chains, and subsequently result of intensification of crystalline imperfection. Furthermore the longer time for mixing the more enough time for EPDM-*g*-MA migrating to HDPE phase and inducing increased degree of crystalline imperfection which displays as the declined T_{c2} value and the enhanced intensity of T_{c2}.

Applied Polymer SCIENCE

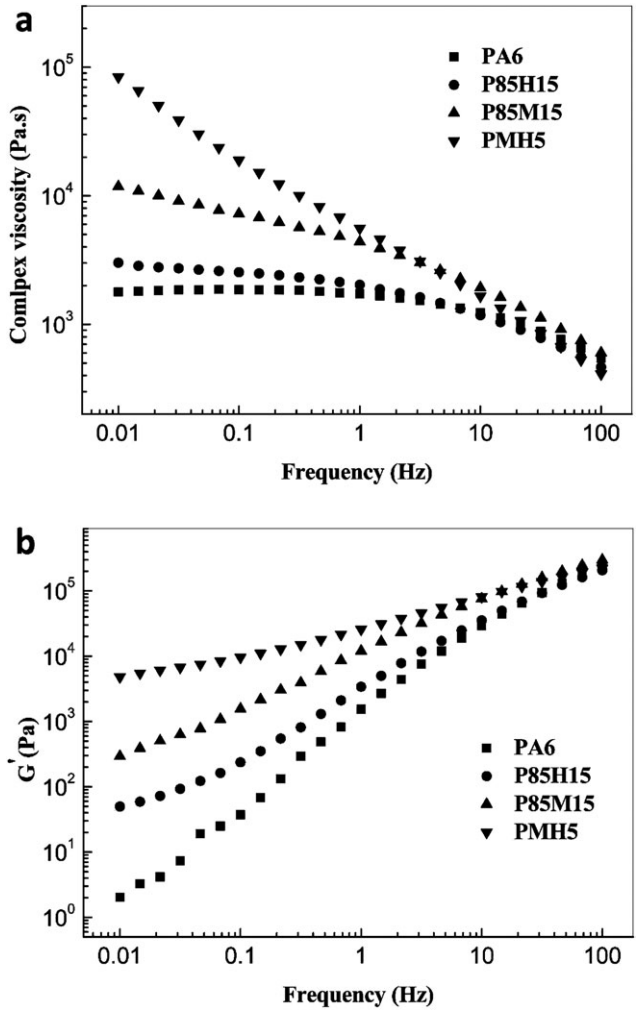

Figure 4. Rheological properties of different blends at 240°C: (a) complex viscosity–frequency curve, (b) storage modulus (G')–frequency curve.

In order to elucidating the special crystallization behaviors of HDPE in ternary blends clearly, more in-depth analyses are required. SSA as a more effectively DSC technology has been employed to analysis the distribution of chain crystallizabilities of semi-crystalline polymers or polymer blend for many researchers.[47–51] The basic principle of SSA thermal fractionation is that crystallization temperature of the chain segment relies on the methylene sequence length since longer methylene chain segments will easily arrange themselves into crystal lattice to form thicker lamellas at higher temperatures and then the lamellas with different thickness will develop a distribution of melting peaks in the final DSC heating scan. So it can be used in our system and give more information about the crystallization behaviors of HDPE phase.

Figure 7 shows the typical DSC heating curve of different blends after SSA thermal fractionation. For all the blends, we can apparently see four separate melting peaks located at the corresponding annealing temperatures of 135°C, 130°C, 125°C, and 120°C, respectively. Furthermore the percentage values of melting area for four distinct peaks are calculated with the method "Gaussian fitting multi-peaks" and the quantitative data are listed in Table III. Compared with the constant temperature of each corresponding peak for all the blends, the melting area for peak 1 and peak 2 separately has a falling and rising tendency from sample PMH2 to PMH15 indicating that the amount of thick and thin lamellas of HDPE phase decreases and increases, respectively. This can be believed that co-crystal forms in the core-shell structure which caused by the entanglement of EPDM-*g*-MA and HDPE molecule chains. Unexpectedly, after analyzing the data of M50H50 (EPDM-*g*-MA/HDPE blends with a composition ratio of 50/50 wt %) listing in Table III, the melting area for peak 1 and peak 2 increases and decrease, respectively. This result is totally different from that in PA6/EPDM-*g*-MA/HDPE blend which indirectly proves that PA6 matrix plays a crucial role on the crystallization behaviors of HDPE.

Hence a novel interpretation for abnormal crystallization behavior of HDPE in ternary blend is proposed in our article. As is well known, shrinkage stresses can be induced in the process of crystallization for semi-crystalline polymer in which has been

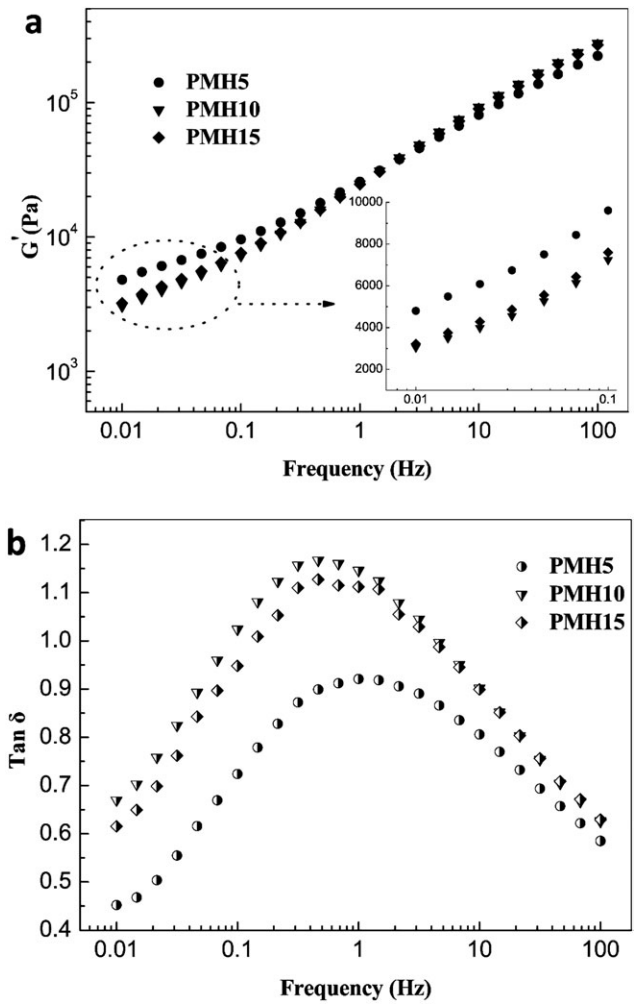

Figure 5. Rheological properties of PA6/EPDM-*g*-MA/HDPE blends at 240°C: (a) Storage modulus (G')–frequency curve, (b) tan δ–frequency curve.

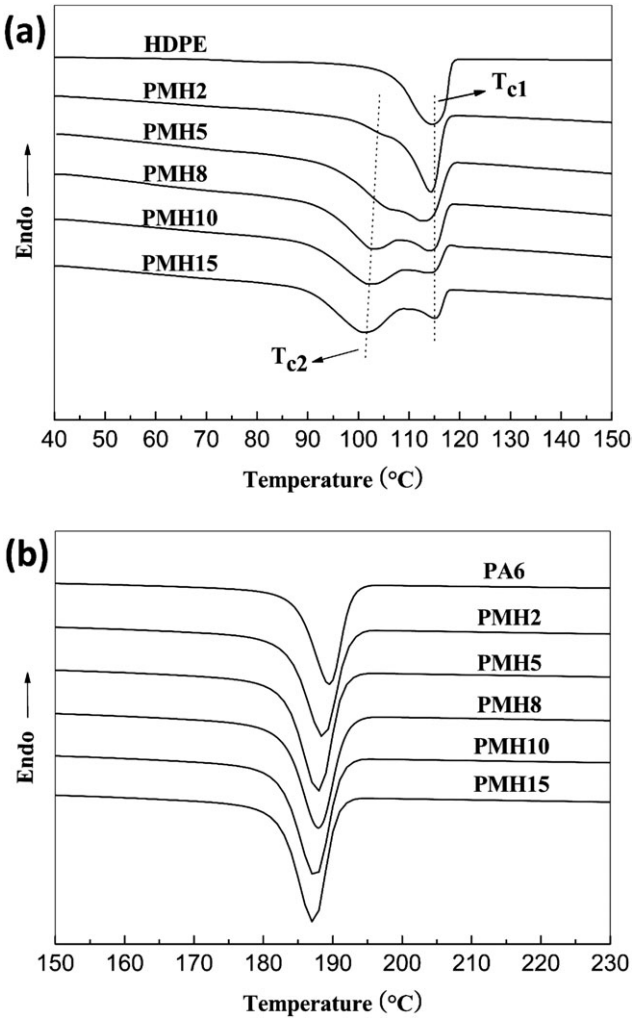

Figure 6. DSC cooling curves show the crystallization behaviors of HDPE component (a) and PA6 component (b) in different blends.

reported by many researchers.[52–55] In our system, the melted core-shell droplets will subject to external pressure being produced from the process of crystalline shrinkage of PA6 matrix because of its high crystallization temperature (seen in Table II). Due to the strong interfacial adhesion between PA6 and EPDM-*g*-MA, the pressure cannot be released by a dewetting process of the interfacial phase and by the formation of interfacial cracks.[54] So under this ambient pressure conditions, the free volume between the molecule chains will be squeezed out leading to reduction of chains motion ability and aggravation of interfacial entanglement of EPDM-*g*-MA and HDPE phase. Along with subsequently cooling, the interfacial entanglement cannot be timely relaxed and the tangled molecule chains are compulsively arranged into the crystal lattice to form co-crystallization after cooling to the crystallization temperature of HDPE phase. Therefore it can be concluded that the abnormal crystallization behavior of HDPE ascribes the aggravation of interfacial entanglement of EPDM-*g*-MA and HDPE inducing by the crystalline shrinkage stress of PA6 matrix.

Crystal Structure

To further understand the crystallization behavior of PA6 and HDPE component in the blends, the crystalline structure was further characterized by using WAXD and the results of selected specimens are shown in Figure 8. Pure HDPE has two intense diffraction peaks at 2θ= 21.4° and 23.7°, corresponding to the (110) and (200) crystal planes, For PA6, it is widely acknowledged that it has two crystal forms, namely α-form and γ-form. In our article, PA6 exhibits two characteristic diffraction peaks at 2θ = 20.3° and 23.4°, attributing to the diffractions of (200) and (002)/(202) planes of α-form. Moreover, the peak at 2θ = 21.2° commonly represents the diffraction of (100) plane of γ-form. Therefore, for PMH5 blend, it is very difficult to distinguish whether the diffraction peak at about 21.2° represents the (110) crystal plane of HDPE or the (100) crystal plane of γ-form of PA6 because they have similar 2θ value. But for P85M15 blend with absence of HDPE phase, peak at 21.2° can be confirmed (100) plane of γ-form of PA6.

Notched Impact Strength

The notched impact strength of pure PA6, pure HDPE and various blends are summarized in Table IV. We can see that the improvement of notched impact strength is greatly dependent of the composition and mixing time. The impact strength of pure PA6 is only 7.3 KJ/m^2 because of its notch-sensitivity and critical brittleness at low temperature which has been reported by Ma etc.[56] For the binary blend of P85H15, the impact strength increases slightly with the addition of HDPE, indicating that HDPE do not promote the fracture toughness for such blend attributing to the distinct polarity and poor interfacial

Table II. DSC Data of Pure Crystallizable Polymers and Its Ternary Blends

	HDPE				PA6		
Blends	T_{c1} (°C)	T_{c2} (°C)	T_m (°C)	X_c (%)	T_c (°C)	T_m (°C)	X_c (%)
PA6	–	–	-	-	190.1	220.3	42.9
HDPE	114.6	-	131.9	61.0	-	-	-
PMH2	114.3	104.9	127.1	48.4	187.1	220.3	30.5
PMH5	114.0	103.8	126.2	46.2	187.8	220.1	31.2
PMH8	114.0	102.2	126.1	43.8	187.9	220.2	30.3
PMH10	114.4	101.3	126.2	42.5	187.5	220.3	31.4
PMH15	114.3	100.7	125.9	39.2	187.2	220.3	32.3

Table III. The Various Parameters of Each Corresponding Melting Peak for Different Blends after SSA Treatment

	Partial melting area (%)			
Blends	Peak 1	Peak 2	Peak 3	Peak 4
Pure HDPE	63.0	26.9	7.8	2.3
M50H50	69.9	18.8	10.1	1.2
PMH2	55.7	31.1	11.6	1.6
PMH5	45.1	39.9	12.5	2.5
PMH8	45.8	38.8	13.4	2.0
PMH10	39.7	43.4	13.9	3.0
PMH15	41.6	43.2	13.0	2.2

adhesion between PA6 and HDPE. In the impact process, these interface defects will accelerate the expansion of micro-cracks and cause premature fracture of the blend.[57] The value of impact strength for P85M15 blend is much higher than that of P85H15 blend, which probably due to the enhanced interaction of PA6 and EPDM-*g*-MA rubber[58] and the formation of more uniform and smaller rubber particles. Considering the ternary blends, however, the impact strength increases greatly with combining the HDPE and EPDM-*g*-MA into the PA6 matrix. For example, PMH8 blend shows an impact strength of 80.7 KJ/m^2, 11 times higher than that of pure PA6 and 3.2 times than that of P85M15 blend, manifesting that the largely toughness of PA6 can be achieved at a low rubber content of 15 wt % which is helpful for reducing the cost of the toughened system. Further increasing the mixing time to 15 min leads to the decrease of impact strength for PMH15 because smaller core-shell particles are apt to agglomerate to form a bigger one [shown in Figure 3(c)]. During the fracture process, the coalescent particles with thin rubber shell are tending to drop out of PA6 matrix which is responsible for the slightly lower toughness compared to the PMH8.

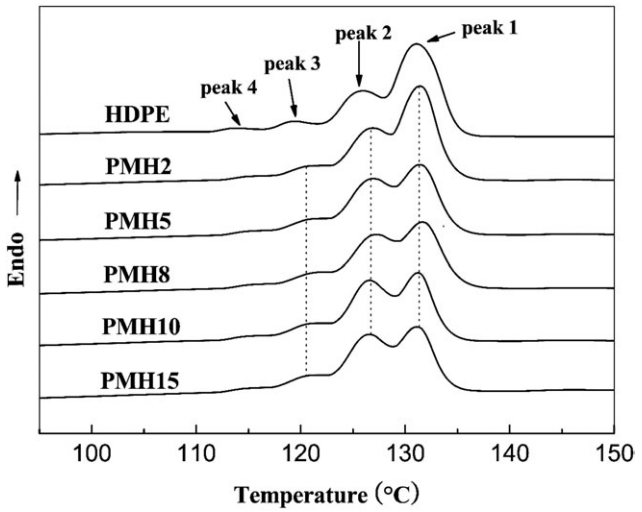

Figure 7. DSC heating curves of different blends after SSA thermal fractionation.

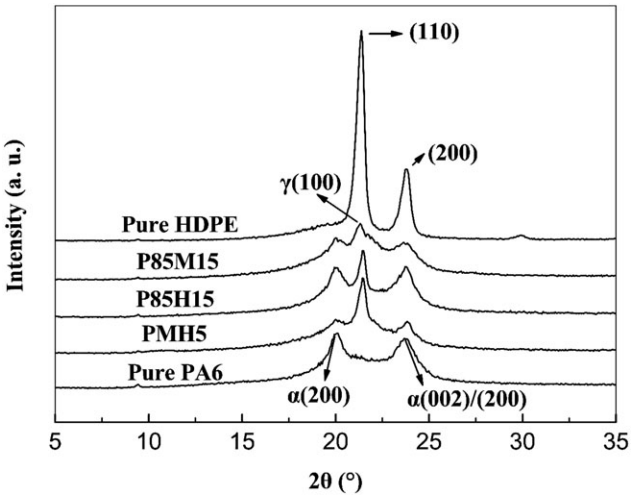

Figure 8. Wide-Angle X-ray diffraction curves of different blends.

All in all, high toughness blends can be still obtained even with longer mixing time (e.g. PMH15 with relatively high impact strength of 66.7 KJ/m^2) compared with both the binary blends. The enhanced Izod impact toughness is mainly caused by the formation of the core-shell structure. We can believe that during the fracture process, the stress is easily to be transferred between HDPE and EPDM-*g*-MA phase through co-crystal structure and between PA6 matrix and core-shell particles through the bridging effect of EPDM-*g*-MA rubber shell. This can be induced more homogeneous distribution of stress and avoiding the severe stress concentration. Also it is evident that the smaller dispersed phase the more interfacial area can be achieved, in which making more chances for EPDM-*g*-MA to migrate into HDPE phase to form co-crystallization or span the PA6 and HDPE phases to obtain strong adhesion between the two phase boundaries, respectively. Hence it can be concluded that the improved toughness for the ternary blends ascribes the two kinds of strong interaction: one is the interface compatibilization of PA6 and EPDM-*g*-MA phase; the other is the co-crystallization of HDPE and EPDM-*g*-MA. In addition, no matter for P85M15 or PMH5 blend, it can be easily found that the both blends have less content of α phase (seen in Figure 8). However, α phase gives higher impact strength than γ phase.[59] Thus the

Table IV. Notched Impact Strength of the Different Blends

Blends	Notched impact strength (KJ/m^2)
Pure PA6	7.3
Pure HDPE	34.0
P85H15	9.6
P85M15	25.6
PMH2	66.5
PMH5	79.8
PMH8	80.7
PMH10	61.7
PMH15	66.7

change of crystalline structure of PA6 matrix has not expressed a positive role on the improvement of impact strength of the ternary blend. Our further work is being carried on to clarify the toughness mechanism thoroughly.

CONCLUSIONS

The effect of core-shell morphology evolution on the rheological behaviors, crystallization, mechanical properties of PA6/EPDM-*g*-MA/HDPE (70/15/15 wt %) blends was investigated. SEM observation shown that core-shell morphology of PA6 as a matrix with HDPE encapsulated within the dispersed EPDM-*g*-MA was obtained after melt-mixing and revealed that the size of dispersed phase domains were gradually changing with mixing time increased. The rheological behaviors of the blends were successful to expound the phase morphology evolution. Specially, DSC studies indicated that co-crystal was formed at the boundaries between EPDM-*g*-MA and HDPE phase which caused by the chain entanglement of the two phases. The PA6/EPDM-*g*-MA/HDPE blends exhibited excellent impact toughness attributing to two kings of strong interface interaction: one was the co-crystal between EPDM-*g*-MA and HDPE, the other was the reactive compatibilization between EPDM-*g*-MA and PA6.

ACKNOWLEDGMENTS

The authors gratefully acknowledge the financial support from the National Key Basic Research Program of China (973 Program, No. 2012CB025902) and the National Natural Science Foundation of China (Contract No. 51273219 and 50903050).

REFERENCES

1. Philip, G.; Hersam, M.; Arnold, M.; Martel, R.; Avouris, A. *Phys. Rev. Lett.* **2001**, *86*, 3128.
2. Lau, K. T.; Hui, D. *Compos. B* **2002**, *33*, 263.
3. Lee, C. F. *Polymer* **2000**, *41*, 1337.
4. Guo, H. F.; Packirisamy, S.; Gvozdic, N. V.; Meier, O. J. *Polymer* **1997**, *38*, 785.
5. Guo, H. F.; Gvozdic, N. V.; Meier, O. J. *Polymer* **1997**, *38*, 4915.
6. Yang, H.; Zhang, Q.; Fu, Q. *Polymer* **2006**, *47*, 2106.
7. Bose, S.; Bhattacharyya, A. R.; Kodgire, P. V.; Misra.A.; Poschke, P. *J. Appl. Polym. Sci.* **2007**, *106*, 3394.
8. Lee, J. K.; Han, C. D. *Polymer* **1999**, *40*, 6277.
9. Favis, B. D. *J. Appl. Polym. Sci.* **1990**, *39*, 285.
10. Favis, B. D.; Therrien, D. *Polymer* **1991**, *32*, 1474.
11. Hobbs, S. Y.; Dekkers, M. E. J.; Watkins, V. H. *Polymer* **1988**, *29*, 1598.
12. Yan, L.; Dong, W.; Zhang, J. M.; Xie, X. M. *Polym. Bull.* **2011**, *66*, 841.
13. Omonov, T. S.; Harrats, C.; Groeninckx G. *Polymer* **2005**, *46*, 12322.
14. Li, L. P.; Yin, B.; Zhou, Y.; Gong, L.; Yang, M. B.; Xie, B. H.; Chen, C. *Polymer* **2012**, *53*, 3043.
15. Li, L. P.; Yin, B.; Yang, M. B. *Polym. Eng. Sci.* **2011**, *51*, 2425.
16. Ha, M. H.; Kim, B. K.; Kim, E. Y. *J. Appl. Polym. Sci.* **2004**, *93*, 179.
17. Kim, B. K.; Kim, M. S. *J. Appl. Polym. Sci.* **1993**, *48*, 1271.
18. Huang, J. J.; Keskkula, H.; Paul, D. R. *Polymer* **2006**, *47*, 624.
19. Huang, J. J.; Keskkula, H.; Paul, D. R. *Polymer* **2004**, *45*, 4203.
20. Reignier, J.; Favis, B. D.; Heuzey, M. C. *Polymer* **2003**, *44*, 49.
21. Horiguchi, S.; Mahcariayakul, N.; Yase, K.; Kitano, T. *Macromolecules* **1997**, *30*, 3664.
22. Liu, H. Z.; Guo, L.; Guo, X. J.; Zhang, J. W. *Polymer* **2012**, *53*, 272.
23. Borggreve, R. J. M; Gaymans, R. J; Schuijer, J.; Ingen Housz, J. F. *Polymer* **1987**, *28*, 1489.
24. Luzinov, I.; Pagnoulle, C.; Jerome, R. *Polymer* **2000**, *41*, 7099.
25. Zhuo, K.; Shi, D.; Yin, J. H.; Li, R.; Mai, Y. W. *Macromolecules* **2008**, *41*, 7264.
26. Tong, C. Y.; Lan, Y.; Chen, Y.; Yang, D. C. *J. Appl. Polym. Sci.* **2011**, *123*, 1302.
27. Paul, D. R.; Bucknall, C. B. Polymer Blends; Wiley-Interscience Publication, Wiley: New York, **2000**.
28. Liu, S.; Qin, S. H.; Luo, Z.; Yu, J.; Guo, J. B.; He, M. J. *Macromol. Sci. Part B: Phys.* **2011**, *50*, 1780.
29. Wang, K. Y.; Chen, Y. M.; Zhang, Y. *Polymer* **2009**, *50*, 1483.
30. Müller, A. J.; Hernandez, Z. H.; Arnal, M. L.; SanchezJ. *J. Polym. Bull.* **1997**, *39*, 465.
31. ASTM D256-05: Standard test method for impact resistant of plastic and electrical insulation materials. *Ann book ASTM stand* **1990**, *8*(1), 57.
32. Gonzaler-Nunez, R.; Arellano, M.; Moscoso, F. J.; Gonzalez-Romero, V. M.; Favis, B. D. *Polymer* **2001**, *42*, 5485.
33. Wang, K.; Wang, C.; Li, J.; Su, J. X.; Zhang, Q.; Du, R. N.; Fu, Q. *Polymer* **2007**, *48*, 2144.
34. Wang, B. B.; Hao, L. X.; Wang W.; Hu, G. S. *J. Polym. Res.* **2010**, *17*, 821.
35. Valera, T. S.; Morita, A. T.; Nicole, R. *Macromolecules* **2006**, *39*, 2663.
36. Bousmina, M.; Muller, R. Rheol. *Acta* **1996**, *35*, 369.
37. Oosterbroek, M.; Waterman, H. A.; Wiseall, S. S.; Altena, E. G.; Mellema, J.; Kip, A. M. *Rheol. Acta* **1980**, *19*, 497.
38. Takano, Y.; Sakanishi, A. *Biorheology* **1982**, *19*, 599.
39. Zhang, Q. H.; Fang, F.; Zhao, X.; Li, Y. Z.; Zhu, M. F.; Chen, D. J. *J. Phys. Chem. B* **2008**, *112*, 12606.
40. Al-Juhani, A. A.; Suleiman, M. A. *Arab. J. Sci. Eng.*; DOI 10.1007/s13369-012-0231-4.
41. Kim, H. B.; Choi, J. S.; Lee, C. H.; Lim, S. T.; Jhon, M. S.; Choi H. *J. Eur. Polym. J.* **2005**, *41*, 679.
42. Krache, R.; Benachour, D.; Potschke, P. *J. Appl. Polym. Sci.* **2004**, *94*, 1976.
43. Tol, R. T.; Mathot, V. B. F.; Groeninckx, G. *Polymer* **2005**, *46*, 369.

44. Tol, R. T.; Mathot, V. B. F.; Groeninckx, G. *Polymer* **2005**, *46*, 383.
45. Tol, R. T.; Mathot, V. B. F.; Groeninckx, G. *Polymer* **2005**, *46*, 2955.
46. Tol, R. T.; Mathot, V. B. F.; Groeninckx, G. *Polymer* **2005**, *46*, 2966.
47. Müller, A. J.; Arnal, M. L. *Prog. Polym. Sci.* **2005**, *30*, 559.
48. Song, S. J.; Wu, P. Y.; Ye, M. X.; Feng, J. C.; Yang, Y. L. *Polymer* **2008**, *49*, 2964.
49. Arnal, M. L.; Canizales, E.; Müller, A. *J. Polym. Eng. Sci.* **2002**, *42*, 2048.
50. Starck, P.; Rajanen, K.; Lofgren, B. *Thermocim. Acta* **2002**, *395*, 169.
51. Sun, X.; Shen, H. W.; Xie, B. H.; Yang, W.; Yang, M. B. *Polymer* **2011**, *52*, 564.
52. Perena, J. M.; Duckett, R. A.; Ward, I. M. *J. Appl. Polym. Sci.* **1980**, *25*, 1381.
53. Chang, R. Y.; Tsaur, B. D. *Polym. Eng. Sci.* **1995**, *35*, 1222.
54. Zhang, Y. C.; Chen, R. Z.; Hui, Z. Z. *J. Adhes. Sci. Tech.* **2000**, *14*, 1405.
55. Jansent, K. M. B.; Titomanlio, G. *Polym. Eng. Sci.* **1996**, *36*, 2029.
56. Ma, L. F.; Wei, X. F.; Zhang, Q.; Wang, W. K; Gu, L.; Yang, W.; Xie, B. H.; Yang, M. B. *Mater. Design* **2012**, *33*, 104.
57. Costantino, C.; Edward, J. K.; Georhes, H. *Macromolecules* **1991**, *24*, 1846.
58. Wang, C.; Su, J. X.; Li, J.; Yang, H.; Zhang, Q.; Du, R. N.; Fu, Q. *Polymer* **2006**, *47*, 3197.
59. Wu, C. J.; Kuo, J. F.; Chen, C. Y. *Polym. Eng. Sci.* **1993**, *33*, 1333.